

Evaluation on Tightly Coupled Integration of GPS PPP and Different Interval IMU Data

Junyao Kan¹, Zhouzheng Gao*¹ and Yu Min¹

¹ School of Land Science and Technology, China University of Geosciences Beijing, Beijing, China

Abstract

Precise point positioning (PPP) has been proved as an effective approach for providing precise positioning services. However, satellite observation outages occur inevitably in the real dynamic application, which leads to partial or complete satellite signal outages and will significantly degrade the accuracy and continuity of PPP positioning. A commonly used approach is to integrate PPP and inertial measurement units (IMU) to enhance the positioning performance. Previous works on this topic are usually based on high sampling rate IMU data. This paper will make an initial assessment of the impacts of different sampling rate IMU data on the tightly coupled integration (TCI) between global positioning system (GPS) and inertial navigation system (INS). After providing the mathematical model of GPS PPP/INS TCI, we investigate the impact of the sampling rate of consumer-grade IMU data under two scenarios (1) original observation scenario; (2) simulation scenario by setting partial satellite signal outage. Results show that (1) the positioning accuracy of the PPP/INS TCI depends on the sampling rate of low-cost IMU data insignificantly when there are enough available satellites; (2) during satellite partial outage periods, the divergent speed of position is visibly affected by IMU sampling rate, and higher positioning accuracy is obtained while setting the IMU sampling rate to 20Hz and 50Hz; (3) the effect of IMU sampling rate on velocity and attitude solutions is also visible, compared with the 200Hz sampling rate, the accuracy of velocity and attitude are improved at 20Hz.

Keywords

Precise Point Positioning, Inertial Navigation System, PPP/INS integration, IMU data rate

1. Introduction

The emerging applications, such as autonomous driving and smart city, present an increasingly urgent demand for high-precision and high-frequency spatial-temporal data information. The Precise Point Positioning (PPP) technique [1], which requires only a single receiver operation, can achieve centimeter-level positioning worldwide with the advantages of flexibility and low cost. Currently, PPP based on Global Positioning System (GPS) observations has been demonstrated as an effective tool for providing high-accuracy location services because of the advantages of GPS' global coverage, all-weather, and non-accumulative positioning error. However, there are GPS challenging environments such as urban canyons, tunnels, and overpass bridges, around where satellites' signals will be blocked. Such conditions make it hard to get continuous and reliable positioning results by using GPS measurements only.

To overcome the drawbacks of GPS, the Inertial Navigation System (INS) is considered to be an effective complementary method. Because INS can provide a stand-alone solution by using the measurements of carrier motion from the Inertial Measurement Unit (IMU). IMU data will not be affected by the surrounding environments. Such character makes INS can cover the shortage of GPS PPP during challenging environments. Nonetheless, it is difficult to maintain high precision positioning for a long time because of the accumulation of IMU sensors' errors over time. Because of

IPIN 2022 WiP Proceedings, September 05–07, 2022, Beijing, China

EMAIL: kanjunyao99@163.com (J. Kan); zhouzhenggao@126.com (Z. Gao); mrminyu123@163.com (Y. Min)

ORCID: 0000-0003-1227-161X (J. Kan)



© 2022 Copyright for this paper by its authors.
Use permitted under Creative Commons License Attribution 4.0 International (CC BY 4.0).
CEUR Workshop Proceedings (CEUR-WS.org)

the complementary characteristics of GPS and INS, the integration of the two systems results in a more reliable, continuous, and accurate higher-rate positioning performance in complex environments.

Generally, the integration of PPP and INS can be classified as Loosely Coupled Integration (LCI) and Tightly Coupled Integration (TCI). As the LCI is based on the solutions of PPP and INS, its performance is determined by INS only during the periods of GNSS satellite partial- and complete-outage. In the TCI models, the pseudo-range and carrier phase observations as range observations are directly combined with the predicted distance of INS, which still can work during GNSS satellite partial-outage periods. Wherein, the TCI performs much better than that of LCI, especially under the GPS signal blocked conditions. Last decades, many works have been done on PPP/INS tight integration and found it can provide decimeter positioning accuracies even when GNSS signals are partially or completely interrupted [2]. Along with the development of the Micro-Electro-Mechanical-Sensors (MEMS) technology, the integration between PPP and MEMS INS has been studied. The works in [3] showed that the LCI and TCI of PPP/MEMS-INS can provide decimeter positioning accuracies. A new approach in [4] is proposed, in which the multi-GNSS PPP and MEMS inertial measurement unit (IMU) is tightly integrated at the observation level. The corresponding results illustrated that the multi-GNSS and INS can enhance the PPP convergence performance visibly. In [5], the tightly coupled integration of ambiguity fixed PPP and MEMS-INS is presented by using a troposphere-constrained adaptive Kalman filter, and centimeter-level positioning accuracy is achieved. However, the above works are based on the high-frequency IMU. Although the high sampling rate of IMU (200Hz) can provide positioning solutions in more detail, it also imposes a certain burden on data storage and operation, which does not meet the application requirements of the consumer-level market in real time.

To meet the demand of the mass-market on location services, it is necessary to evaluate the performance of the positioning method with low-cost hardware, small data storage, and non-time consuming operation. Therefore, this paper is to investigate the effect of consumer-grade IMU data sampling rate on GPS PPP/INS tight integration in terms of positioning accuracy, velocity accuracy, and attitude accuracy. In this contribution, the uncombined undifferenced PPP is introduced into the tightly coupled integration, and it is evaluated by a set of vehicle-borne data.

2. First level heading

In this paper, the PPP/INS tight integration system is applied based on Extend Kalman Filter (EKF) [5]. The corresponding details are described as follows.

2.1. State model

The state function of PPP/INS tight integration can be expressed as

$$X_k = \Phi_{k,k-1} X_{k-1} + \mu_{k-1}, \mu_{k-1} \sim N(0, Q_{k-1}) \quad (1)$$

where $\Phi_{k,k-1}$ denotes the state transition matrix for the state parameter vector X_k ; μ_{k-1} is the state noise vector with the apriori variance Q_{k-1} .

For the TCI model, the corresponding state parameters used in our work can be written as [7]

$$X_{TCI} = [\delta p_{INS}^n, \delta v_{INS}^n, \delta \Psi, \delta B_a, \delta B_g, \delta S_a, \delta S_g, \delta t_r, \delta i_r, \delta d_{wet}, \delta DCB_r, \delta N_1, \delta N_2, \delta I_r]^T \quad (2)$$

where δp_{INS}^n , δv_{INS}^n , and $\delta \Psi$ are the correction vectors of position, velocity, and attitude in the navigation (n) frame respectively; δB_a and δB_g represent the bias error of accelerometer and gyroscope; δS_a and δS_g represent the scale factor error of accelerometer and gyroscope. The remaining part is the state parameters related to PPP; δt_r and δi_r are the correction of clock offset and drift of receiver; δd_{wet} is the residual of the zenith total delay of the tropospheric wet component; δDCB_r is the correction of receiver hardware time delay in terms of Differential Code Bias (DCB);

δN_1 and δN_2 denote the ambiguity error on frequency L1 and L2; δI_r represent the ionospheric delay correction along the signal transmitting path.

The so-called PSI angle model [8] is used to describe the dynamic changes of position, velocity, and attitude, which can be defined as

$$\left. \begin{aligned} \delta \dot{\mathbf{p}}^c &= -\boldsymbol{\omega}_{ec}^c \times \delta \mathbf{p}^c + \delta \mathbf{v}^c \\ \delta \dot{\mathbf{v}}^c &= \mathbf{f}^c \times \boldsymbol{\psi} + \mathbf{C}_b^p \delta \mathbf{f}^b - (\boldsymbol{\omega}_{ie}^c + \boldsymbol{\omega}_{ic}^c) \times \delta \mathbf{v}^c + \delta \mathbf{g}^c \\ \dot{\boldsymbol{\psi}} &= -\boldsymbol{\omega}_{ic}^c \times \boldsymbol{\psi} - \mathbf{C}_b^p \delta \boldsymbol{\omega}_{ib}^b \end{aligned} \right\} \quad (3)$$

where $\delta \mathbf{p}^c$, $\delta \mathbf{v}^c$, and $\boldsymbol{\psi}$ indicate the position, velocity, and attitude error in the computing frame (c -frame) respectively; $\boldsymbol{\omega}_{ec}^c$ is the angular rate of the c -frame relative to the earth frame (e -frame) projected in c -frame; $\boldsymbol{\omega}_{ie}^c$ is the rotation angular rate of e -frame with respect to the inertial frame (i -frame) projected in the c -frame; $\delta \mathbf{g}^c$ represents the gravity error in c -frame; \mathbf{f}^c is the specific force from accelerometers; \mathbf{C}_b^p represents the attitude direction cosine matrix for transforming from body frame (b -frame) to platform frame (p -frame), and “ \times ” denotes the cross-product; $\delta \boldsymbol{\omega}_{ib}^b$ and $\delta \mathbf{f}^b$ represent the sensor errors of accelerometers and gyroscopes.

In addition, the first-order Gauss-Markov process [9] is used to depict the residuals of IMU sensor errors, which can be expressed as:

$$\begin{bmatrix} \delta \dot{B} \\ \delta \dot{S} \end{bmatrix} = \begin{bmatrix} -\delta B / T_B \\ -\delta S / T_S \end{bmatrix} + \begin{bmatrix} \omega_B \\ \omega_S \end{bmatrix} \quad (4)$$

where δB and δS represent the bias and scale factor, T_B and T_S are the correlation time of IMU sensor errors; ω_B and ω_S are the driving white noise of bias and scale factor errors respectively.

For the parameters related to GNSS, the random walk process is adopted to represent the dynamic behavior of the receiver clock offset/drift, the residual of zenith troposphere delay in the wet component, the receiver hardware time delays, and the ionospheric delays, and the random constant model is used to describe the changes of ambiguities. Then, the state transition matrix of the TCI can be achieved finally.

2.2. Measurement model

The measurement model for the TCI can be written as

$$\mathbf{Z}_k = \mathbf{H}_k \mathbf{X}_k + \boldsymbol{\eta}_k, \boldsymbol{\eta}_k \sim N(\mathbf{0}, \mathbf{R}_k) \quad (5)$$

where \mathbf{Z}_k and \mathbf{H}_k denote the innovation vector and the design matrix at epoch k for state parameter vector \mathbf{X}_k ; $\boldsymbol{\eta}_k$ stands for the observation noise vector with the covariance matrix \mathbf{R}_k .

The innovation vector is formed by making differential operations between GPS observations and INS predicted values

$$\mathbf{Z}_{TCI,k} = \begin{bmatrix} P_j \\ L_j \\ D_j \end{bmatrix} - \begin{bmatrix} P_{j,INS} \\ L_{j,INS} \\ D_{j,INS} \end{bmatrix} = \begin{bmatrix} P_j - \|p_s - p_{INS} - \Delta p_{INS,j}\| - \Delta P_j \\ L_j - \|p_s - p_{INS} - \Delta p_{INS,j}\| - \Delta L_j \\ D_j - \|v_s - v_{INS} - \Delta v_{INS,j}\| - \Delta D_j \end{bmatrix} \quad (6)$$

where P , L , and D indicate the raw observations of pseudo-range, carrier-phase, and Doppler at frequency j , respectively; ‘INS’ represents the INS predicted values; p_s and v_s are the satellite position and velocity calculated by GPS precise orbit/clock products; p_{INS} and v_{INS} are the position and velocity at the IMU center predicted by INS mechanization; ΔP , ΔL , and ΔD refer to the sum of corrections of pseudo-range, carrier-phase, and Doppler, respectively; $\Delta p_{INS,j}$ and $\Delta v_{INS,j}$ are the lever-arm between the measuring centers of GNSS receiver and that of IMU, which can be written as [10]

$$\begin{pmatrix} \Delta p_{INS,j} \\ \Delta v_{INS,j} \end{pmatrix} = \begin{pmatrix} C_n^e C_b^n l^b \\ C_n^e [(\boldsymbol{\omega}_{in}^n \times) C_b^n l^b + C_b^n (l^b \times) \boldsymbol{\omega}_{ib}^b] \end{pmatrix} \quad (7)$$

where C_n^e is the transition matrix between e -frame and n -frame; C_b^n denotes the transition matrix between n -frame and b -frame; l^b represents the lever-arm values measured in b -frame; $\boldsymbol{\omega}_{in}^n$ indicates

the rotation angular rates of n -frame with respect to i -frame projected in n -frame; ω_{ib}^b is the angular rate in b -frame.

Then, we can get the designed coefficient matrix H_k can be obtained by making an error perturbation operation on the innovation vector in Eq. (6) around the initial state parameters provided by INS mechanization.

2.3. Algorithm implementation

According to the above mathematical models, the PPP/INS tightly integration solution can be received by adopting EKF. Figure 1 shows the implementation of TCI. After the initialization for EKF, the INS mechanization worked by using the compensated IMU outputs and provided INS-updated position, velocity, and attitude. Then, the time update phase is run based on the state function to achieve the predicted state parameter and the corresponding variance. Afterward, time synchronization between GPS observations and IMU data at the current IMU epoch is adopted to determine whether the Kalman measurement update working or going to the next IMU epoch. Finally, the navigation solutions from INS are then corrected with the estimated navigation error parameters by a closed-loop feedback process.

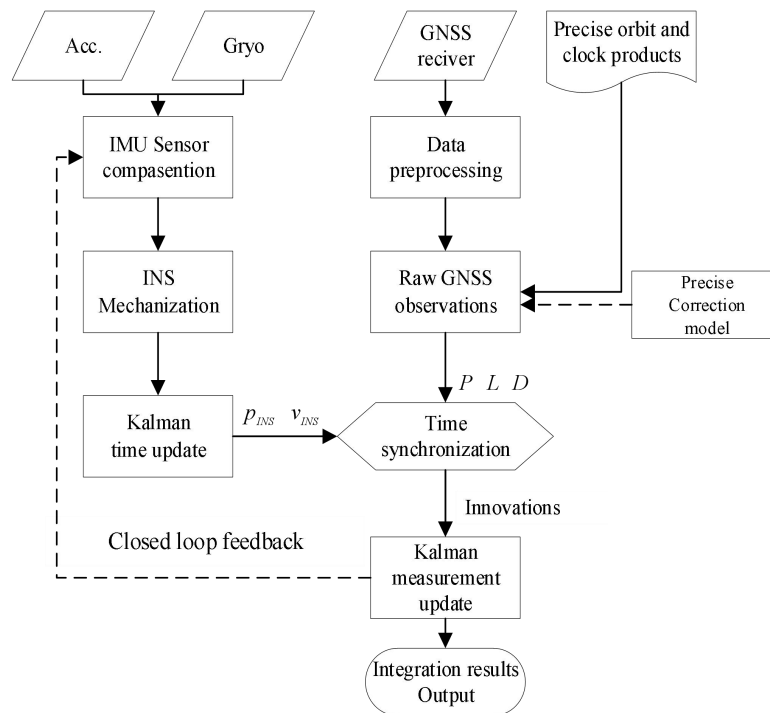


Figure 1: Implementation of PPP/INS tightly coupled integration

3. Experiments And Discussions

3.1. Experiment and Data Processing Schemes

To evaluate the performance of PPP/INS tightly integration as well as the impacts of IMU sampling rate on the TCI results, a set of vehicle-borne data collected around Wuhan China is processed. Figure 2 shows the detailed trajectory of the experiment. The test is arranged in an urban environment with a maximum speed of 10 m/s. A Trimble NetR9 receiver, a high-grade IMU POS1100 (gyro bias instability of 8 °/h), a consumer-grade IMU ICM-20602 (gyro bias instability of 50 °/h) were equipped. The sampling rates of the GPS observations and IMU measurements were 1Hz and 200Hz, respectively. In addition, the basic information about the IMU sensor is listed in Table 1.

In this paper, the raw GPS observations and the data from four IMU were processed in PPP/INS TCI mode. Meanwhile, the raw 200Hz IMU data is re-sampled to 100Hz, 50Hz, and 20Hz. To further evaluate the impacts of IMU sampling rate on the accuracy of positioning, velocity, and attitude determination while suffering GNSS signals outages, two groups of 30-second partial satellite signal outages were simulated. To assess the performance of the above schemes, the smoothed solutions from RTK/POS1100 tight integration were employed as reference values. The number of available satellites and the PDOP value for GPS are shown in Figure 3. The number of available satellites is almost about 6~7 and it drops to 4 under some GPS difficult environments.



Figure 2: Trajectory of the vehicle test.

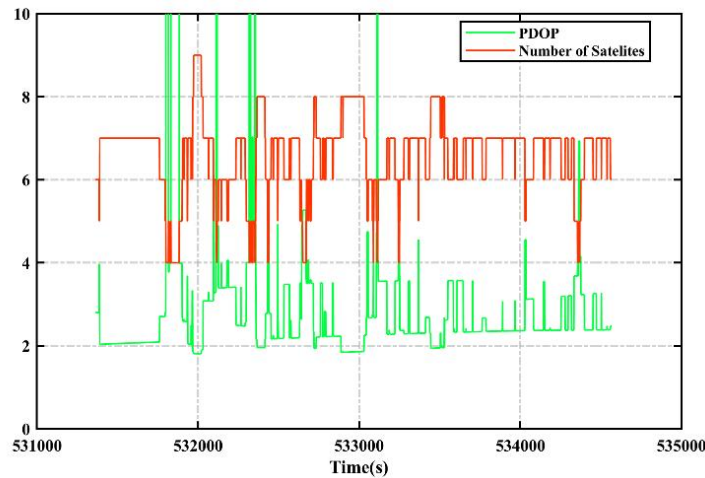


Figure 3: Number of available satellites and the corresponding PDOP.

Table 1

Details of CONSUMER-GRADE IMU Sensor

Parameters	Values
IMU grade	MEMS
Gyroscope bias ($^{\circ}/h$)	50
Accelerometer bias (mGal)	250
Angular random walk ($^{\circ}/\sqrt{h}$)	0.24
Velocity random walk ($m/s/\sqrt{h}$)	0.24

3.2. Impacts of IMU data interval on PPP/INS integration

The position differences of PPP/INS tightly integration calculated by four types of IMU data (200Hz, 100Hz, 50Hz, and 20Hz) compared to the reference values are shown in Figure 4. For comparison, the PPP position solutions based on uncombined undifferenced GPS data were also provided. The position accuracy in terms of Root Mean Square (RMS) values is listed in Table 2. Significantly, the results of PPP/INS TCI are more accurate than that of PPP. Using IMU data at a 200 Hz sampling rate, the TCI position RMSs are 7.59 cm, 19.53 cm, and 55.51 cm in east, north, and up directions, with the improvements percentages of 26.2%, 51.1%, and 27.7%, respectively. While using IMU measurements at different sampling rates, this brings 0.63 cm, 2.34 cm, and 3.79 cm position differences in terms of RMS in the north, east, and vertical directions among the four IMU data based on PPP/INS TCI. According to Table 2, there are 0.8%, 5.8%, and 3.5% three-dimensional position improvements for the PPP/INS TCI based on 100Hz, 50 Hz, and 20Hz IMU data, respectively compared with those based on 200Hz IMU data. However, there no significant relationship exists between position accuracy and the reducing the IMU data sampling rate.

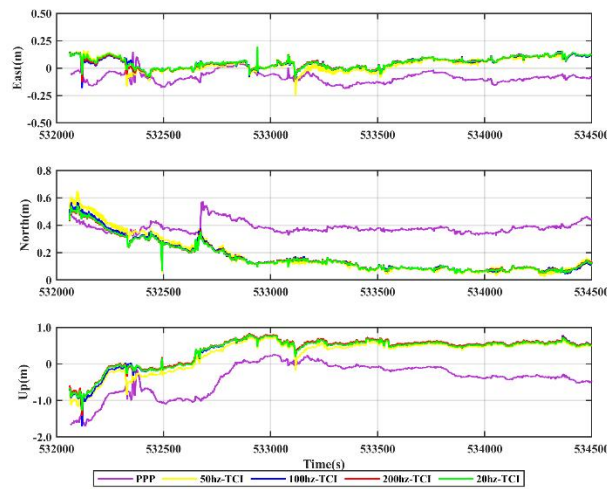


Figure 4:Position differences of PPP and PPP/INS TCI by using four types of IMU data (200Hz, 100Hz, 50Hz, and 20Hz).

Besides, we also analyze the accuracy of velocity and attitude while using IMU data at different sampling rates. The time series of velocity and attitude differences with respect to the references are shown in Figure 5 and Figure 6, respectively. The corresponding RMSs are shown in Table 2. Significantly, compared with the results using IMU data at a 200Hz sampling rate, the accuracy of velocity and attitude are both degraded by using IMU data at 100Hz and 50Hz. There is an improvement while using 20Hz IMU data. According to the statistics, the velocity and attitude accuracies at 50Hz are the lowest. Wherein, the velocity RMSs are about 6.12 cm/s, 5.62 cm/s, and 2.02 cm/s in east, north, and up components, and that of attitude are about 0.602°, 0.805°, and 3.911° for roll, pitch, and heading, respectively. In addition, the velocity RMSs based on 20Hz IMU data are 2.10 cm/s, 1.85 cm/s, and 2.08 cm/s, and that of attitude are 0.103°, 0.129°, and 1.021° for roll, pitch, and heading, respectively.

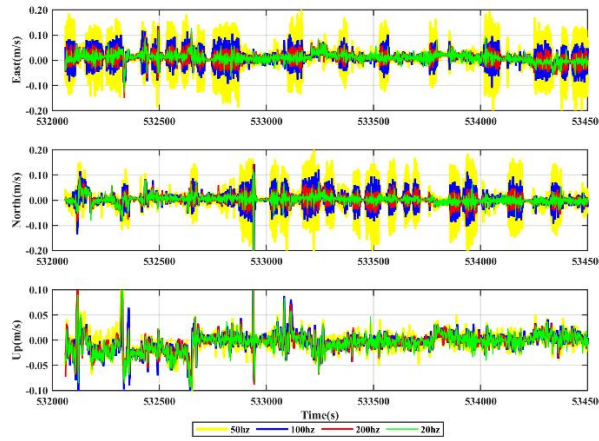


Figure 5:Velocity differences of PPP/INS TCI by using four types of IMU data (200Hz, 100Hz, 50Hz, and 20Hz).

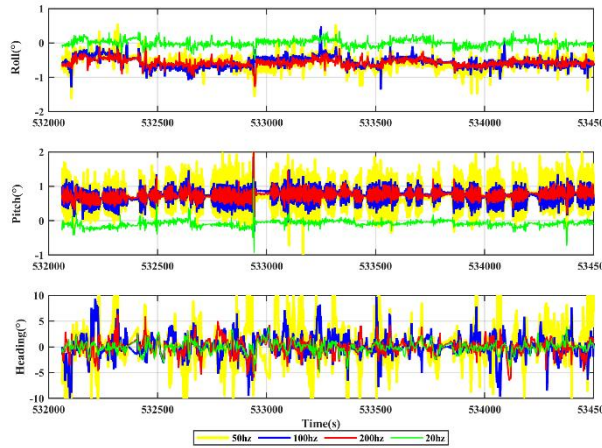


Figure 6:Attitude differences of PPP/INS TCI by using four types of IMU data (200Hz, 100Hz, 50Hz, and 20Hz).

Table 2
RMS of position, velocity, and attitude

Mode	Position (cm)			Velocity(cm/s)			Attitude (°)		
	East	North	Up	East	North	Up	Roll	Pitch	Heading
PPP	10.28	39.93	76.81						
TCI-200Hz	7.59	19.53	55.51	2.44	2.18	1.97	0.581	0.738	1.466
TCI-100Hz	6.96	20.59	54.90	3.43	3.15	1.98	0.588	0.776	2.181
TCI-50Hz	7.12	21.87	51.72	6.12	5.62	2.02	0.602	0.805	3.911
TCI-20Hz	7.23	20.01	53.37	2.10	1.85	2.08	0.103	0.129	1.021

To further evaluate the performance of PPP/INS tightly coupled integration in complex conditions, we simulate the GNSS raw observations by setting two 30-second partial satellite signal outages at 532768 s and 533798 s. During each partial outage period, only three satellites are available. Simultaneously, IMU data with different sampling rates (200Hz, 100Hz, 50Hz, and 20Hz) are processed to further investigate the impacts of IMU sampling rates on TCI during GNSS challenging environments. Figure 7 illustrates the position solutions of PPP and TCI using four types of IMU data, and the corresponding RMSs are listed in Table 3. Visibly, the PPP/INS tightly coupled integration can obtain continuous positioning results even if there are not enough GNSS observations for PPP (during 532768 s~532798 s and 533798 s~533828 s). According to the statistics in Table 3, the position

accuracy enhancements are 38.9%, 56.8%, and 35.4% in the east, north, and up while using IMU data at 200Hz sampling rate (10.35 cm, 20.26 cm, and 51.60 cm) compared to that of PPP (16.94 cm, 4.88 cm, and 80.82 cm). Similar position enhancements compared with the solutions of PPP can also be found while using the IMU data at a different rate. Comparing the position RMSs calculated by using different rate IMU data, the RMS differences are not remarkable with the maximum values of 0.09 cm, 0.16 cm, and 4.98 cm. Similarly, there is also no strong relationship between positioning accuracy and the IMU data rate. However, obvious position convergence can be found during the GPS outages.

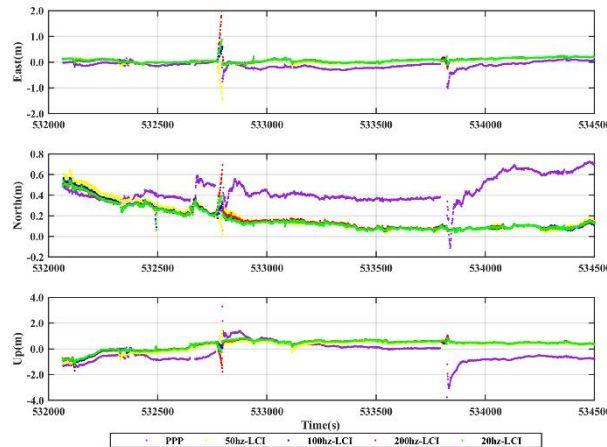


Figure 7:Position differences of PPP and PPP/INS TCI by using GNSS simulation data and four types of IMU data (200Hz, 100Hz, 50Hz, and 20Hz).

Figure 8 and Figure 9 show the solutions of velocity and attitude calculated by PPP/INS TCI using the satellite partial outage simulation GPS data and different sampling rate IMU data. The corresponding RMSs are listed in Table 3. Results indicate that there are no significant impacts of the 30-second GPS partial outages on the velocity and attitude solutions can be found. It is mainly due to the high-accuracy character of INS during a short time. Besides, the influences of different IMU sampling rates on the velocity and attitude accuracy are much more visible than that of position.

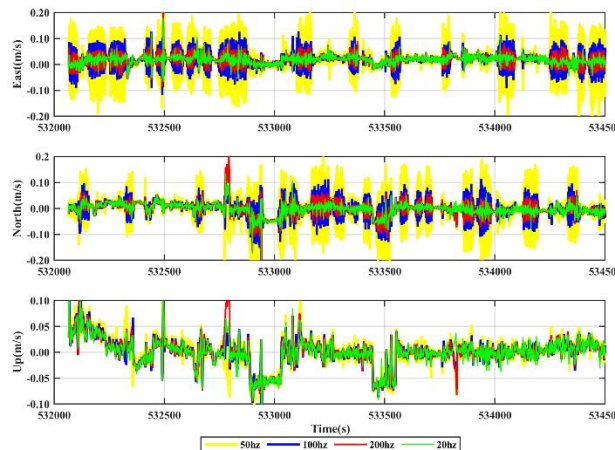


Figure 8:Velocity differences of PPP/INS TCI by using GNSS simulation data and four types of IMU data (200Hz, 100Hz, 50Hz, and 20Hz).

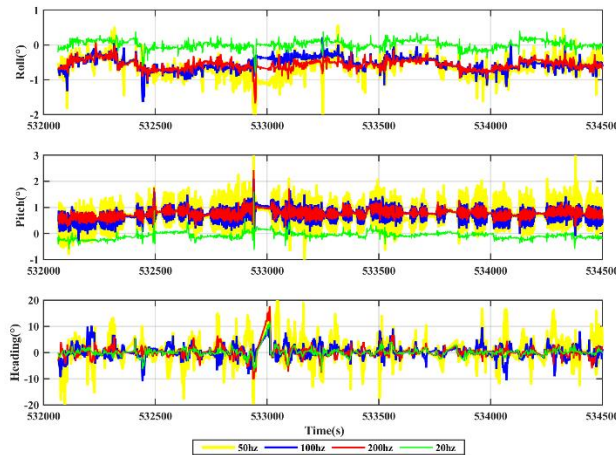


Figure 9: Attitude differences of PPP/INS TCI by using GNSS simulation data and four types of IMU data (200Hz, 100Hz, 50Hz, and 20Hz).

Table 3
RMS of position, velocity, and attitude

Mode	Position (cm)			Velocity(cm/s)			Attitude (°)		
	East	North	Up	East	North	Up	Roll	Pitch	Heading
PPP	16.94	46.88	80.82						
TCI-200Hz	10.35	20.26	51.60	2.79	2.64	2.70	0.585	0.762	2.22
TCI-100Hz	10.32	20.66	52.09	3.75	3.59	2.80	0.576	0.792	2.47
TCI-50Hz	10.37	22.28	47.11	6.52	6.25	2.94	0.692	0.831	4.62
TCI-20Hz	10.41	20.12	51.28	2.43	2.34	2.70	0.127	0.155	1.57

Position drifts calculated by four types of IMU data during the outages are given in Figure 10, the maximum position errors are shown in Figure 11. Significantly, it can be seen that the position drifts of PPP/INS TCI diverge along with outage time. The position RMS while using 200Hz IMU data is degraded to 143.6 cm, 37.30 cm, and 141.3cm in east, north, and vertical directions while partial outage time lasts 30 s. However, the position drifts are restrained while using lower sampling rates. Among the results calculated from different rate IMU data, the position drifts after 30 s outage are improved to 34.20 cm, 20.03 cm, and 53.67 cm in east, north, and up directions while using IMU data at 100Hz. The maximum position drifts for 50Hz IMU data are 80.30 cm, 21.170 cm, and 115.30 cm and those for 20Hz are 55.02 cm, 25.09 cm, and 60.99 cm, respectively. It shows significantly that IMU sampling rate affects position drifts of PPP/INS TCI when there are satellite partial outages. In general, for consumer-grade IMU ICM-20602, the positioning results will diverge rapidly over time. Nevertheless, it is equivalent to reducing IMU sensor cumulative error by reducing INS mechanization frequency while downsampling IMU data rate. In addition, although there are position improvements when using low sampling rate (100Hz, 50Hz, and 20Hz) IMU data, such improvements do not present a significant positive correlation with IMU data rate. What is also evident is that the position drifts of PPP/INS TCI during the GNSS partial outage show a better positioning accuracy in the north component than in the other two directions.

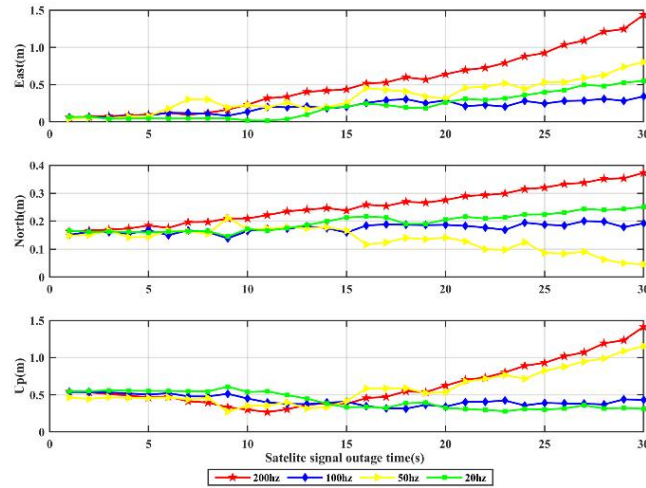


Figure 10: RMSs of position drifts computed by PPP/INS TCI using four types of IMU data with different sampling rates in the GNSS outage simulation test.

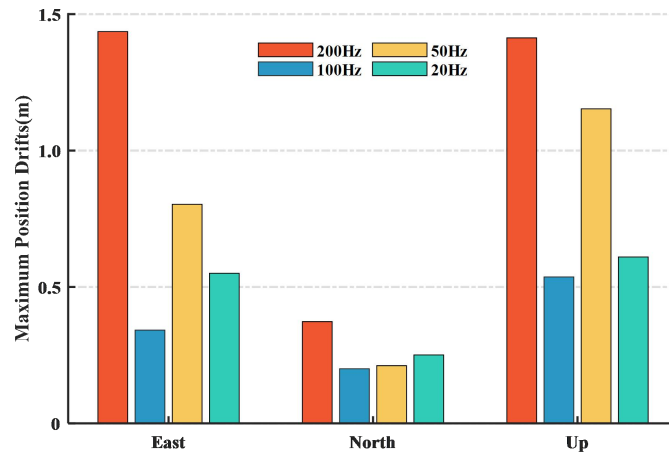


Figure 11: Maximum position drifts of PPP/INS TCI during GNSS outage simulation period.

4. Conclusion

In this paper, the impacts of IMU data interval on the performance of the tightly coupled integration between PPP and INS are evaluated by a set of vehicle-borne data. Moreover, we provide the GPS partial satellite outages simulation to furtherly evaluate the performance of PPP/INS tightly coupled integration in unexpected urban conditions. According to the results, the positioning accuracy of PPP/INS TCI is significantly improved compared with that of the stand-alone PPP approach when using both original data and simulation data. In addition, the effect of the IMU sampling rate on position accuracy is inconspicuous when the satellite signals are available for PPP. It is due to that the absolute positioning accuracy of PPP/INS TCI mainly depends on PPP. However, the position error drifts along with the increasing outage time, and such divergent speed is visibly affected by the IMU sampling rate.

5. Acknowledgements

Many thanks to GNSS Research Center, Wuhan University for providing GPS/INS vehicle-borne data. This study is funded by the National Key Research and Development Program of China (Grant No. 2020YFB0505802).

6. References

- [1] J. Zumberge, M. Heflin, D. Jefferson, M. Watkins, and F. Webb, "Precise Point Positioning For The Efficient And Robust Analysis Of GPS Data From Large Networks," *Journal Of Geophysical Research: Solid Earth*, vol. 102, no. B3, 1997, pp. 5005-5017.
- [2] E. Shin and B. Scherzinger, "Inertially Aided Precise Point Positioning," in *Proceedings of the 22nd International Technical Meeting of the Satellite Division of The Institute of Navigation*, 2009, pp. 1892-1897.
- [3] S. Du, *Integration of Precise Point Positioning and Low-Cost MEMS IMU*. Calgary: University of Calgary, 2010
- [4] Z. Gao, H. Zhang, M. Ge, X. Niu, W. Shen, J. Wickert, and H. Schuh, "Tightly Coupled Integration Of Multi-GNSS PPP And MEMS Inertial Measurement Unit Data," *GPS Solutions*, vol. 21, no. 2, 2016, pp. 377-391.
- [5] H. Han, T. Xu, and J. Wang, "Tightly Coupled Integration Of GPS Ambiguity Fixed Precise Point Positioning And MEMS-INS Through A Troposphere-Constrained Adaptive Kalman Filter," *Sensors*, vol. 16, no. 7, 2016, p. 1057.
- [6] R.G. Brown, and P.Y. Hwang, *Introduction to random signals and applied Kalman filtering*. Wiley, 1992.
- [7] Z. Gao, *Research on the methodology and application of the integration between the multi-constellation GNSS PPP and inertial navigation system*. China: Wuhan University, 2006.
- [8] E. Shin, *Estimation techniques for low-cost inertial navigation*. Canada: University of Calgary, 2005
- [9] R.G. Brown, and P.Y. Hwang, *Introduction To Random Signals And Applied Kalman Filtering*. Willey, 1997.
- [10] Z. Gao, M. Ge, W. Shen, Y. Li, Q. Chen, H. Zhang, and X. Niu, "Evaluation On The Impact Of IMU Grades On BDS + GPS PPP/INS Tightly Coupled Integration," *Advances In Space Research*, vol. 60, no. 6, 2017, pp. 1283-1299.